A Method for estimate of range variation of attenuation from dual frequency and dual polarization radar

-Validation using scattering database of snow-

Takahisa Kobayashi

Takahisa Kobayashi[1,2] , Mistuharu Nomura[1] ,Soichiro Sugimoto[1],Ahoro Adachi[2],

Nobuhiro Nagumo[2] and Hiromaru Hirakuchi[1].

[1]*Central Research Institute of Electric Power Industry,1646,Abiko,Chiba,Japan,270-1194*
[2]*Meteorological Research Institute, Tsukuba, Japan, 305-0035*

(Dated: 22 June 2018)

1 Introduction

An accurate measurement of snow is one of important topics to be solved in the radar meteorology. The relationships between the equivalent radar reflectivity (Ze) and snowfall rate (s) differs significantly from Ze-r (r: rainfall rate) for rain. In addition, the Ze-s relationship varies significantly with snow type, drysnow, wet snow, mixed-phase precipitation etc. Classification of hydrometeors is, as a first step, needed for quantitative precipitation estimation from Z-r(s) relationship. Traditionally, snow areas are identified from ambient temperature and relative humidity (e.g., Matsuo and Sasyo, 1981). Many hydrometeor classification methods for dual-polarization radars have been also developed (e.g., Kouketsu et al., 2015, Chandrasekar et. al., 2013). Most methods use the polarimetric radar signatures such as reflectivity (Ze), differential reflectivity (Zdr), specific differential phase (Kdp), and the correlation coefficient between horizontal and vertical Ze (ρ_{HV}) measured at each radar resolution volume. These parameters often have similar values for different types of precipitation and it is needed to identify the type of precipitation by combining above signatures.

For reflectivity-based rainfall rate estimate, the specific attenuation is an amount to be removed from radar received signals. Many extensive studies have, therefore, focused on the attenuation correction. Attenuation is closely related to rainfall rate and therefore, methods of rainfall rate estimate based on attenuation properties have been developed (Matrosov, 2005, Ryzhkov et al., 2014). Although attenuation is relatively insensitive to the drop size distribution (DSD), the specific attenuation also depends on the type of precipitation. The attenuation of dry snow is generally small at most radar frequencies. While for rain, large attenuations appear. It has also been reported that melting hail has very large attenuation (Thurai et al., 2015).Hydrometeor classification is also needed in the attenuation-based rainfall estimate. In other words, attenuation can be a useful information for hydrometeor classification.

There are no straightforward methods for accurate estimate of attenuation. Most methods to estimate attenuation utilize redundancy relations among radar observables. The specific attenuation (A) can be estimated if A is related to the intrinsic radar reflectivity factor (Ze^t) by a power law (Hitshchfeld and Bordan, 1954). This method was modified by using path-integrated attenuation (PIA) which was used in rainfall rate estimate algorithm in the radar equipped on the Tropical Rainfall Measuring Mission (TRMM) (Meneghini and Nakamura, 1990, Iguchi and Meneneghini, 1994). This method was further modified for the dual frequency space-borne radar (DPR) onboard the Global Precipitation Mission (GPM).

For dual-polarization radars, a linear relationship between the path integrated attenuation (PIA) and the differential phase (Φdp) has been used to estimate attenuation (Bringi et al., 1990, Ryzhkov et al., 2014).The redundancy has been also used for attenuation correction (Adachi et al., 2013, 2015). These methods are useful, however, the coefficients in the relationships between Φdp and A significantly differ, depending on particle size distribution, precipitation type, and temperature.

To avoid the variation of the coefficients, We have developed a method by using changing tendency of the radar variables in the radar propagation path instead of the variables at each radar resolution volume (Kobayashi et al., 2015). The method estimates radar range variations of the relative values of attenuation from the dual frequency ratio (DFR) which is defined as the difference of Ze at a frequency of Ku and Ka measured with the DPR. We have also developed a similar method for a dual-polarization radar (Kobayashi et al., 2017). Both methods intend to classify rain and dry snow and have been examined by simulations based on the T-matrix method. In the simulation, snow particles are assumed to be spheroidal shape. This assumption may not be appropriate for radar operated at higher frequency.

In this presentation, we examined the methods for attenuation estimate by simulations using scattering database for irregular snow by Lu et al. (2016).The objective of our study is to examine the methods for snow of irregular shape and for severe conditions of snow to estimate of snow, i.e., snow of large scattering and small attenuation.

2. Methods for attenuation estimate

For dry snow, the attenuations are generally negligible. For rain, on the other hand, large attenuations appear. In our methods, the different attenuation properties are used to hydrometeor classification. As mentioned earlier, attenuation is closely related to specific differential phase (Kdp) as $A=\alpha Kdp$. The coefficient α significantly depends on type of precipitation as well as temperature. To avoid the effects of variation of α, we use the range variation of the radar received signals instead of values at specified ranges. The methods, therefore, do not estimate attenuation at specified range but at some region of radar range in which no significant changes in precipitation properties exist. We estimate attenuation for hydrometeor classification from the relative magnitude of attenuation in the radar propagation path (Fig.1). We have developed two method; one is for a dual-frequency radar and another is for a dual-polarization radar(Kobayashi et al., 2015, 2017).

Fig.2.1 Schematic figure of hydrometeor classification from range variation of attenuation.

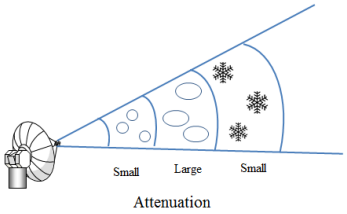

2.1 Methods for attenuation estimate from dual frequency radar (MAD)

The DPR onboard the GPM core satellite operates at frequencies of Ku-band (14GHz) and Ka-band (35GHz). The dual frequency ratio (DFR) is obtained from the DPR and is defined as,

$$DFR = Z_e(Ku:dBZ) - Z_e(Ka:dBZ). \qquad (2.1.1)$$

For rain of small size of raindrops, the scattering properties both at Ka and Ku-band radar are in the Rayleigh regime, which results in small values of the DFR unless attenuation is significant. For rain of large size of raindrops, the scattering properties at Ka-band radar is in the Mie regime but are still in the Rayleigh regime at Ku-band radar, which results in larger value of DFR. For snow, on the other hand, the scattering properties are in the Mie regime both for Ka and Ku-band radar. Larger size of particles generally lead to larger values of DFR. DFR associated with the different scattering properties of particles between Ka and Ku-band is called here as 'scattering effect' (DFRs). The different scattering effect can be used to classify hydrometeor type from measurements by using the Dual-frequency precipitation radar (Liao, and Meneghini, 2011). Their method, however, neglects attenuation and therefore needs exact attenuation correction.

In addition to the scattering effects, attenuation due to rain results in increases in DFR. Larger attenuation of the radio wave in rain, in general, occurs at higher radar frequencies. Attenuation due to rain is not significant for Ku-band but is significant for Ka-band. This different attenuation property enhances DFR. For dry snow, attenuation can be usually neglected both for Ka and Ku-band radar. It should be mentioned that "dry snow" is defined here as pure ice snow which is composed of ice and air. DFR associated with the different attenuation is related to rain rate and drop size and is called here as 'attenuation effect'. For dry snow, DFR is determined by only the scattering effects because of almost no attenuation at both 35 and 14 GHz. While for rain, DFR is determined by both the scattering and the attenuation effects. The path integrated attenuation (PIA) increases with total rain rate in the propagation path. Thus, larger decreasing tendency of the measured reflectivity factor in the propagation path should appear at higher frequencies for homogeneous precipitation. The differential PIA between Ka and Ku-band is defined here as the attenuation effects (DFRa), which monotonically increase with the path integral rain rate if the DFRs is constant in the propagation path.

$$DFRa = PIA(Ku) - PIA(Ka) = \int_{r1}^{r2} \int_{d\min}^{d\max} [\sigma_a(Ku) - \sigma_a(Ka)]N(D)dDdr, \qquad (2.1.2)$$

Here, σ_a is attenuation coefficient. A key factor for hydrometeor classification is the attenuation effects which tend to enhance DFR and appear only in precipitation with attenuation like rain.

$$DFR = DFR_s + DFR_a, \quad \text{for rain.} \qquad (2.1.3)$$

$$DFR = DFR_s, \quad \text{for dry snow.}$$

We can, therefore, identify the medium as rain if we can detect DFRa in the measured DFR (DFRm). To detect DFRa, we should firstly remove DFRs from DFRm.

The scattering effects are basically related to the size of particles. Large values of DFRs arise primarily from large particles in size. The increases in the size of particles are, generally, associated with higher precipitation rate, ie. Larger values of Ze at Ku-band. **T**herefore, the DFRs can be expected to increase with intrinsic value of Ze.

Figure 2.2 shows the relationship between DFRs and intrinsic value of Ze (Ze^t) at Ku-band for rain. The DFRs increases with Ze^t(Ku) linearly. For mixed phase precipitation, the DFRs also tends to increase with Ze^t(Ku) (Fig.2.2). Thus, we assume that the DFRs is related Ze^t by power law as,

$$DFR_s = cZe^{t\,d}, \qquad (2.1.4)$$

Coefficients c and d depend on precipitation type. The ratio of the DFR to Ze^{td}(Ku) is given by

$$Dz \equiv DFR / Ze^{t\,d} = c + DFRa / Ze^{t\,d}, \qquad (2.1.5)$$

The parameter Dz is, therefore, a measure of the DFRa. We assume that Ze^t(Ku) can be approximated as measured value Ze(Ku). Figure 2.3 shows the ratio of the DFR to Ze(Ku) versus the DFRa. The ratio is linearly related to the DFRa except for DFR/Ze<0.1. Although the coefficients c and d varies with snow properties of the volume equivalent diameter D_0, density etc., the T-matrix calculations suggests that the relationship of Eq.2.1.4 is generally valid at Ze (Ku) larger than 10-20dBZ (Liao and Meneghini, 2005). Here the coefficient b was assumed to be 1. The derivative of DFRa with range shows attenuation per unit length of range.

$$\frac{dDz}{dr} \equiv \left(\frac{dDFRa}{dr} Ze^d - DFRa \frac{dZe^d}{dr} \right) / dZe^{2d} \approx, \frac{dDFRa}{dr} / Ze^d \qquad (2.1.6)$$

For snow of low density, the DFRa is generally smaller than the DFRs. Large contributions of DFRs to DFR need accurate estimate of DFRs. For dry snow, we assume Ze(Ku) as Ze(Ka)=c'$Ze^{d'}$(ku) in linear scale instead of Eq. 2.1.4. Figure 2.4 shows the relationship between Ze^t(Ka) versus Ze^t(Ku) in linear scale for aggregate snow by using the scattering database by Lu et al. (2016).

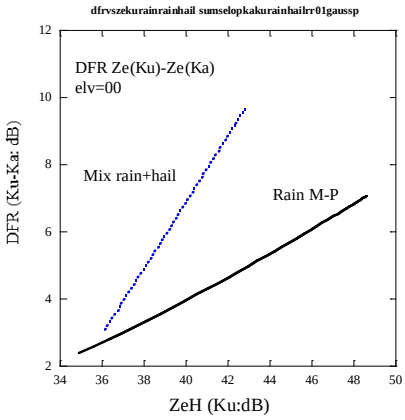

Fig.2.2 DFRs versus Ze(Ku) for rain and mixed-phase precipitation.

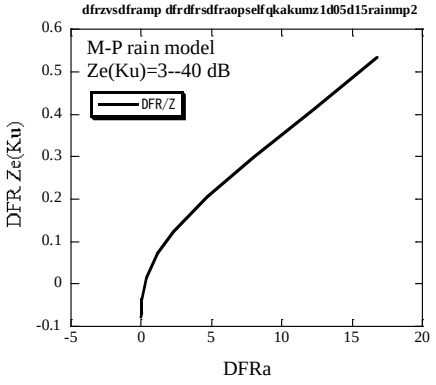

Fig.2.3 DFRs /Ze(Ku) versus DFRa for rain.

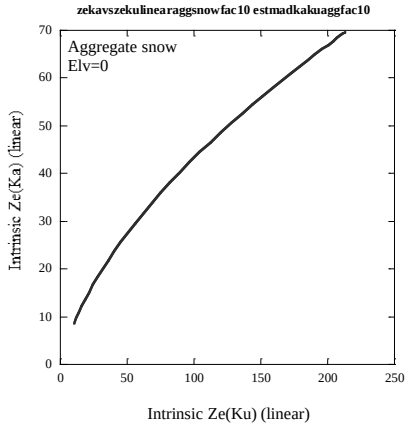

Fig.2.4 Ze^t(Ku) versus Ze^t(Ku) in linear scale for aggregate snow.

2. 2 Method for attenuation estimate from dual polarization radar (MAP)

As mentioned earlier, the attenuation was estimated from the range variation of the DFR calculated from Ze at Ku and Ka-band which have different propagation effect, that is, different attenuation. Similar technique can be applied for a single frequency dual-polarization radar. Various polarization radar signatures have different attenuation effects. Larger attenuation effects appear in the horizontally polarized reflectivity (ZeH) than the vertically polarized (ZeV) for rain of oblate raindrops. The specific differential phase Kdp is not affected by attenuation. We can, therefore, estimate attenuation from the range variation of parameters with different propagation effects.

One-way path-integrated attenuation at range r in linear scale (PIA^L) is given by

$$2PIA^L(r) = Z_e^t(r) - Z_e^m(r). \qquad (2.2.1)$$

Here, Z_e^t is 'intrinsic' (no attenuated) radar reflectivity, and Z_e^m is the measured reflectivity in linear scale. We assume that Z_e^t is related to Kdp by power law) as

$$Z_e^t(r) = aKdp^b. \qquad (2.2.2)$$

From (2.21) and (2.2.2), the path integrated attenuation is given by

$$2PIA^L = aKdp^b - Z_e^m(r). \qquad (2.2.3)$$

Devided by Kdp, (2.2.3) is given by,

$$Q_Z \equiv \frac{2PIA^L}{Kdp^b} = \frac{aKdp^b - Z_e^m}{Kdp^b} = a - \frac{Z_e^m}{Kdp^b}. \qquad (2.2.4)$$

The parameter Qz is related to attenuation. The specific attenuation (Ad) of the difference of Ze can be obtained by taking derivative of (2.2.4) in terms of range assuming that the coefficient of *a* is constant in the range of dr.

$$Ad(\Delta r) = \frac{dPIA^L}{dr} = -Kdp^b \frac{dQ_Z(r)}{2dr} \qquad (2.2.5)$$

or

$$Ad(\Delta r) = -Kdp^b \frac{Q_Z(r+\Delta r) - Q_Z(r)}{2\Delta r} \qquad (2.2.6)$$

In taking derivative, coefficients *a* and *b*, and Kdp are assumed to be constant in the region of range Δr. The unknown term *a* is therefore removed and is the advantage of this method.The shorter length of Δr is better for the assumption of constant values of coefficient a and Kdp. However, larger Δr is better for deriving less noisy Kdp. The coefficient *b* is unknown and is taken to be 1 in this study. We intend to derive range variations of the relative value of attenuation (Fig.2.1), therefore the incorrect value of *b* is not serious unless large variation of *b* in the propagation path Δr. Although, backscattering effect on Kdp may not negligible for X-band radar (Matrosov, 1999, Troomel, et al.,2013), we neglect the effects in the simulation because exact theoretical calculation of the scattering effect is still uncertain (Oguchi T., personal communications).

This method is based on the relationship between Kdp and Ze as shown in Eq.2.2.2. For rain, similar relationships have been reported (eg, Bringi et al., 1990). This is because axis ratio of raindrops is larger for larger size of raindrops. This assumption is therefore reasonable for rain. Figure 2.4 shows the simulation plots of Kdp versus Ze^t at X and C-band for rain of the M-P size distribution. Figure2.5shows the simulation plots of Kdp versus Ze^t at X and C-band for mixture of rain of the M-P size distribution and spherical ice particles. Linear relationships between log(Kdp) and Ze^t(Ku) are obtained both for rain and mixed-phase precipitation. For mixed-phase precipitation, similar relationships have been reported by Balakrishnan and Zrnic (1990). Figure 2.6 shows plots of Kdp versus Ze^t(Ku) at X and C-band for wet snow simulated with the T-matrix method. The shape of snow particles is assumed to be oblate with the axis ratio of 1.6. The refractive index of snow particles was calculated with the Maxwell-Garnet theory. The water fraction varies 0 to 20 percent in volume with range. Linear relationships clearly appear. This method, so called soft oblate model, is a less time consuming simulation process and is useful for studies on polarimetric scattering of snow. The scattering properties calculated from the soft oblate model is different from the correct values of irregular and complex shape of snow. The observed specific differential phase has not clearly related to Ze at C-band (Ryzhkov and Zrnic, 1998). This is because complicated properties of the relation among shape, size,and densities of snow particles and small values of Kdp at C-band for snow. Fortunately, larger values of Kdp appear for radar of higher frequency. We examined the Kdp-Ze relationship for realistic shape of snow particles by using the scattering database for irregular snow particles developed by Lu et al. (2016). Figure 2.7 shows the relation for aggregate snow of M-P size distribution.. Linear relationships can be obtained.

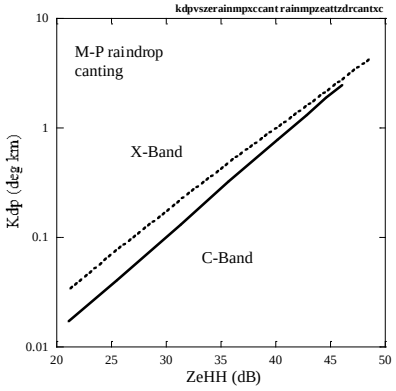

Fig.2.4 Simulation plots of Kdp versus Ze^t at X and C-band for rain of the M-P size distribution.

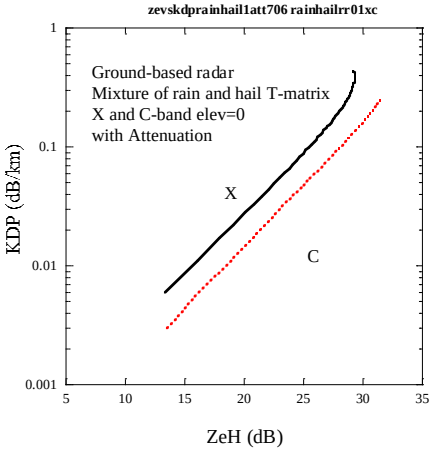

Fig.2.5 Same as Fig.2.4 but for mixed-phase precipitation of rain and hail.

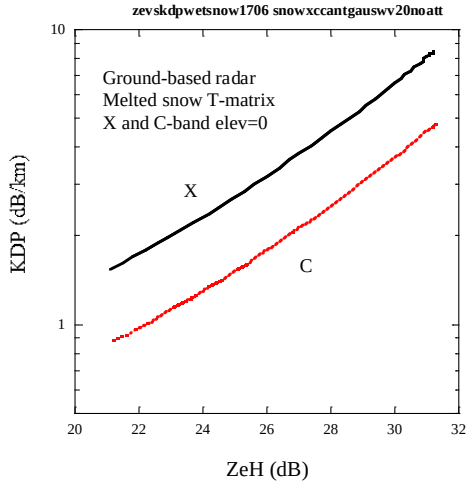

Fig.2.6 Simulation plots of Kdp versus Ze^t at X and C-band for wet snow calculated using T-matrix method.

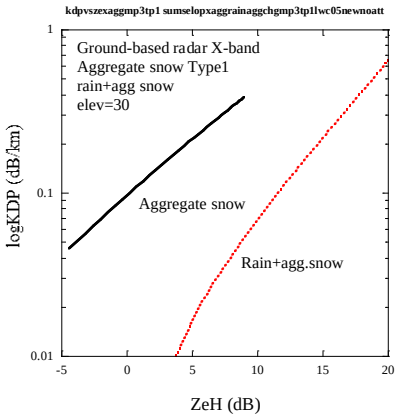

Fig.2.7 Simulation plots of Log(Kdp) versus Ze^t at X and C-band for aggregate snow.

3. Validations: simulations for aggregate snow

Two methods for estimate attenuation, MAD and MAP have been examined by simulation for rain, snow and mixed-phase precipitation (Kobayashi et al., 2016, 2017). In the simulation, scattering properties of raindrops, ice particles and snow particles were calculated with the radar simulator using T-matrix method (Kobayashi et al., 2011). The shape of such hydrometeors was assumed to be oblate. The refractive index for snow is calculated using the Maxwell-Garnett mixing formula associated with various water fraction in snow. The T-matrix approaches have been widely used for snow of complicated shape and are useful for studies on interpretation of radar signals. The scattering properties of irregular snow particles of large size calculated with the T-matrix approach may be , however, inappropriate at higher frequencies of radio wave (Tyynela et al., 2011).

The scattering properties of irregular snow have been calculated using various numerical technique like the Discrete Dipole Approximation (DDA) and have been arranged into a database (Lu et al., 2016, Kuo et al., 2016). Here, we will examine the MAD and MAP by using the scattering database for dry snow by Lu et al. (2016). Attenuation of dry snow is generally negligible. The specific attenuation of snow in the database shows very small in x and Ku-band (Fig.3.1). Even for Ka-band, attenuation is too small to examine the method for estimate attenuation properties for small values of snowfall rate. Thus, we calculate scattering properties of aggregate snow of high snow fall rate. Gaussian range variations of snowfall rate at the maximum of 10 mm/h at the range of 10km are applied. The maximum value may be too high for real snow but for suitable for the validation test.

3.1 MAD

As show in Eq.2.1.4, DFRs is assumed to be due to related to Ze(Ku) as DFRs=cZe^d(Ku). This assumption is appropriate for relatively large attenuated precipitation. Figure 3.2 shows the range variations of Range variations of Ze(Ka), Ze(Ku) and DFR for aggregate snow. The DFR does not tend to increase with range monotonically. This is because large contribution of DFRs to DFR. This is because small attenuation and large reflectivity associated with high snowfall rate of dry snow. To derive DFRa, more accurate estimate of DFRs is needed. We assume relationship as Ze(Ka)= c'Ze$^{d'}$(Ku) in linear scale instead of the relation of DFRs=cZe^d(Ku) [dB].

$$Ze(Ka) = cZe^d \quad [\text{linear} \quad \text{scale}], \qquad (3.1)$$

Figure 3.3 shows the range variations of DFR/Ze^d(Ku) as well as Ze(Ka), Ze(Ku) in linear scale. Parameter *d* is taken to be 0.3. Monotonically increase tendency of DFR/Ze^d(Ku) with range appears. Figure 3.4 shows the results of estimate. The method successfully estimate range variation of attenuation even for snow of large scattering contribution to DFR.

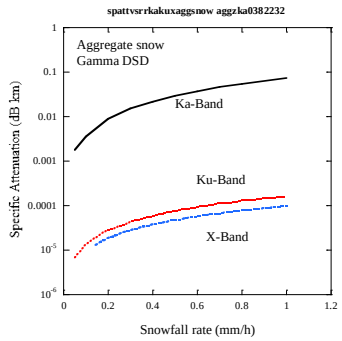

Fig.3.1 Specific attenuations of aggregate snow at Ka, Ku and X-band.

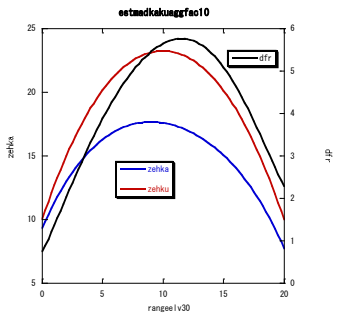

Fig.3.2 Range variations of Ze(Ku), Ze(Ka) and DFR/Ze(Ku) for aggregate snow.

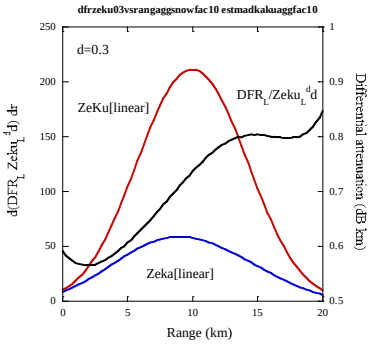

Fig.3.3 Range variations of Ze(Ka) Ze(Ku) and DFR/Ze^d(Ku) in linear scale.

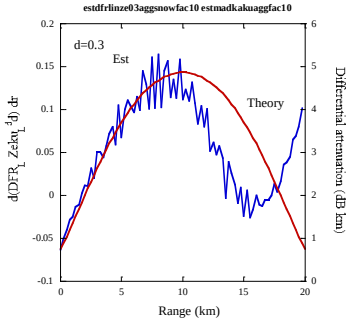

Fig.3.4 The range variation of estimated attenuation and theoretical value for aggregate snow.

3.2 MAP

Figure 3.5 shows the range variation of the intrinsic reflectivity factor (Ze^t) and attenuated value (Zem). Although snowfall rate is the maximum at the range of 10km, the peak of the reflectivity factor Zem is around 8 km because of attenuation. Difference between Ze^t and Zem has a peak at range of 10km and decrease with range associated with largest scattering at 1range of 10km. Figure 3.6 shows the range variation of Q_Z and Kdp. The parameter Q_Z tends to monotonically increase with the range except for short range region in which small values of Kdp. The assumption Eq.2.22 is proved to work well for estimate attenuation for aggregate snow.

Figure3.7 shows the range variation of estimated relative specific attenuation of difference of ZeH (Ad) (solid line) and the theoretically calculated value (dotted line) for aggregate snow. Although there are slight differences at larger radar range, the overall tendencies of the range variation are in good agreement. It should be mentioned that the coefficient b is taken to be 1, therefore, the estimated attenuation is a relative value. The overestimated attenuations appear at range of smaller than 2 km and larger than 17km are associated with errors in the assumption of Eq. 2.1.4. Overall, the method successfully estimate range variation of attenuation even for snow of small attenuation and large scattering properties.

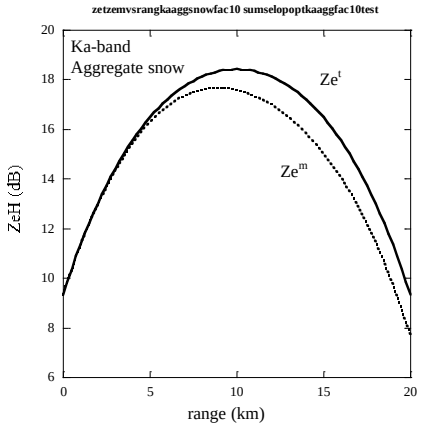

Fig.3.5 Intrinsic value of Ze versus Kdp for aggregate snow.

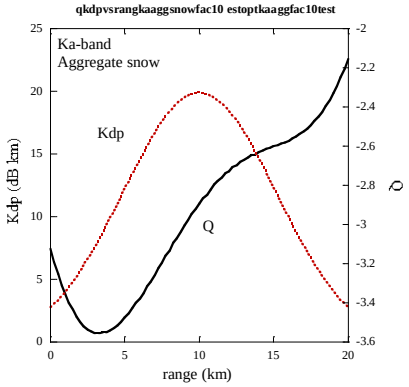

Fig.3.6 The range variation of Q_Z andZe for aggregate snow.

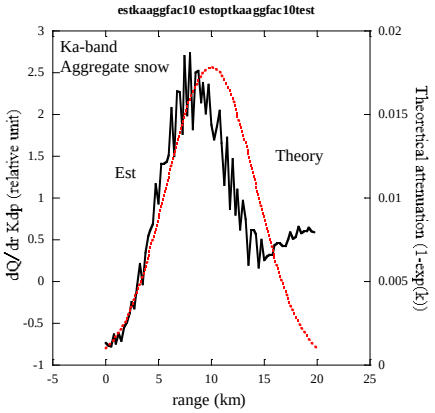

Fig.3.7 The range variation of estimated attenuation and theoretical value for aggregate snow.

4. Summary

We have developed methods to estimate range variation of attenuation from single polarization radars at ka and Ku-band, and a dual polarization radar. We have already examined the methods for rain and snow of spheroidal shape. In this paper, we have examined the methods for aggregate snow by using scattering data base for irregular shape of snow by Lu et al. (2016). Results show that the estimated range variation of attenuation f agrees with the theoretical calculations for aggregate snow. Both methods, MAD and MAP can successfully estimate range variation of attenuation even for severe condition of precipitation to estimate attenuation, that is, snow of large scattering and small attenuation. These methods are useful for precipitation classification from GPM DPR and dual polarization radar. These methods are also useful for more accurate precipitation classification with current classification method.

References

Adachi, A., T. Kobayashi, and H. Yamauchi, 2015: Estimation of raindrop size distribution and rainfall rate from polarimetric radar measurements at attenuating frequency based on the self-consistency principle. *J. Meteor. Soc. Japan*, **93**, 359-388.

Adachi, A., Kobayashi, T., Yamauchi, H., and Onogi, S., 2013: Detection of potentially hazardous convective clouds with a dual-polarized C-band radar. *Atmos. Meas. Tech.*, **6**, 2741-2760.

Balakrishnan, N., and D. S. Zrnic, 1990, Estimation of rain and hail rates in mixed-phase precipitation, J. Atmos. Sci., 47, 565-583. Kobayashi,T., and K. Masuda, H. Yamauchi, and A. Adachi, 2011, Physically-based Simulator for measurements of precipitation with Polarimetric and Space-borne Radars, SPIE Remote Sensing, Cheko, Praha 9/18-9/24, 2011.

Bringi, V. N., and V. Chandrasekar, N.Balakrishnan, D.S. Zrnic, 1990, An examination of propagation effects in rainfall on radar measurements at microwave frequencies, J. Atmos. Oceanic Technol., 7,829-840.2001:Kobayashi T., M. Nomura ,S. Sugimoto, F. Akimoto Furuzawa, A, Adachi, and H. Hirakuchi, 2015: Radar simulation studies for dual-frequency radar measurements of snow from space: Hydrometeor classification. Extended Abstract, 37th Conf. on Radar Meteor., Amer. Meteor.Soc., 108.

Chandrasekar, et.al., 2013, Recent advamces in classification of observations from dual polarization weather radars. *Atmos. Res.*, 119, 97-111

Hitschfeld, W., and J. Bordan, 1954: Errors inherent in the radar measurement of rainfall at attenuating wavelengths. *J. Meteor.* **11,** 58–67.

Iguchi, T., and R. Meneghini, 1994: Intercomparison of single-frequency methods for retrieving a vertical rain profile from airborne spaceborne radar data. *J. Atmos. Oceanic Technol.,* **11,** 1507–1516.

Kobayashi, T. ,M. Nomura ,S. Sugimoto,A. Adachi, N. Nagumo and H. Hirakuchi.2017,Radar simulation studies for hydrometeor classification from range profile of polarimetric radar signatures,Extenden abstract 38th Conf. on Radar Meteor., Amer. Meteor. Soc., 1-10.

Kobayashi, T., S. Sugimoto, M. Nomura and A. Adachi、2015, Radar simulation studies for measurement of precipitation from space-borne radar on GPM、Extended Abstract, Conference on Radar in Meteorology and Hydrology 2014. Extended abstract,

Kouketsu, T. et al., A,2015, A hydrometeor classification method for X-band polarimetric radar: Construction and validation focusing on solid hydrometeors under moist environments, *J. Atmos. Oceanic. Technol.*, 32, 2052-2074.

Kuo, K.-S., and Coauthors, 2016: Themicrowave radiative properties of falling snow derived from nonspherical ice particle models. Part I: An extensive database of simulated pristine crystals andaggregate particles, and their scattering properties. *J. Appl. Meteor. Climatol.*, 55, 691–708, doi:10.1175/JAMC-D-15-0130.1.

Liao, L., and R. Meneghini, 2011, A study on the feasibility of dual-wavelength radar for identification of hydrometeor phases, *J. Appl. Meteor. Clim*, 50, 449-456

Lu, Y. et al., 2016, A polarimetric scattering database for non-spherical ice particles at microwave wavelengths, Atmos. Meas. Techniques, 9, 5119-5134.

Matrosov, S., et al., 1999: Prospects for measuring rainfall using propagation differential phase in X- and Ka-radar bands, *J. Appl. Meteor*., 38,766-776.

Matrosov, S., 2005: Attenuation-based estimate of rainfall rates aloft with vertically pointing Ka-band radars. *J. Atmos. Oceanic Technol*., 22,43-54.

Matsuo, T. and Y. Sasyo, 1981, Melting of snow flakes below freezing level in the atmosphere. *J. Meteorl. Soc. Japan*, 59, 10-24.

Meneghini, R., and K. Nakamura, 1990: Range profiling of the rain rate by an airborne weather radar. *Remote Sens. Environ.*, **31,** 193–209.

Ryzhkov, A., and D. S, Zrnic, 1998: Discrimination between rain and snow with polarimetric radar, *J. Appl. Meteor*., 37,12281240.

Ryzhkov, A., M. Diederich,P.,.Zhang, C. Simmer,2014: Potential utilization of specific attenuation for rainfall estimation,mitigation of partial beam blockage, and radar networking, *J. Atmos. Oceanic Technol*., 31,599-619.

Thurai, M., E. Chobanyan, V.N. Bringi and B.M. Notaroš, 2015, Large raindrops against melting hail: calculation of specific differential attenuation, phase and reflectivity, ELECTRONICS LETTERS ,. 51, 1140–1142

Tromel, S., M. R. Kumjian, A. V., Ryzhkov, C. Simmer, and, M. Diederich, 2013: Backscatter differential phase estimation and variability. *J. Appl. Meteor. Climatol.*, 52,2529–2548

Tyynela, J., J.Leinonen, D. Moisseev, and T. Nousianen, 2011, Radar backscattering from snowflakes: comparison of fractal, aggregate, and soft spheroidal model, *J. Atmos. Oceanic Technol*., 28、1365-1372.